Chapter 17
Nonlinear Aeroelasticity, Flight Dynamics and Control of a Flexible Membrane Traction Kite

Allert Bosch, Roland Schmehl, Paolo Tiso and Daniel Rixen

Abstract This chapter presents a computational method to describe the flight dynamics and deformation of inflatable flexible wings for traction power generation. A nonlinear Finite Element approach is used to discretize the pressurized tubular support structure and canopy of the wing. The quasi-steady aerodynamic loading of the wing sections is determined by empirical correlations accounting for the effect of local angle of attack and shape deformation. The forces in the bridle lines resulting from the aerodynamic loading are imposed as external forces on a dynamic system model to describe the flight dynamics of the kite. Considering the complexity of the coupled aeroelastic flight dynamics problem and the Matlab®implementation, simulation times are generally low. Spanwise bending and torsion of the wing are important deformation modes as clearly indicated by the simulation results. Asymmetric actuation of the steering lines induces the torsional deformation mode that is essential for the mechanism of steering. It can be concluded that the proposed method is a promising tool for detailed engineering analysis. The aerodynamic wing loading model is currently the limiting factor and should be replaced to achieve future accuracy improvements.

17.1 Introduction

In contrast to the rotor blades of a conventional wind turbine, inflatable membrane wings as used for Airborne Wind Energy (AWE) conversion are lightweight and highly flexible. As consequence, the shape of these wings is determined by complex

Allert Bosch · Roland Schmehl (✉)
Delft University of Technology, Faculty of Aerospace Engineering, Kluyverweg 1, 2629HS, Delft, Netherlands, e-mail: r.schmehl@tudelft.nl

Paolo Tiso · Daniel Rixen
Delft University of Technology, Faculty of Mechanical Engineering, Mekelweg 2, 2628CD, Delft, Netherlands

aeroelastic phenomena which result from the interaction of flow-induced forces on the wing surface and the internal structural forces in the membrane fabric, which essentially are tensile and shear forces. Because of the low inertia, the structure responds to control commands, fluctuations of the apparent wind velocity and other changes of geometry or boundary conditions. On the other hand the boundary conditions of the FSI problem continuously change as the relative flow conditions vary along the flight trajectory. Previous research has shown that spanwise torsion plays an important role for the high maneuverability of C-shaped kites [2]. Other aeroelastic phenomena which can sometimes be observed during flight, such as oscillatory bending of the entire wing ("jellyfishing") or flapping of the wing tips, are generally decreasing the aerodynamic performance.

To further improve the design of kite power systems in terms of performance and safety characteristics, high-fidelity computer models of inflatable membrane wings are indispensable. This is not only important for developing a detailed understanding of the dynamic behavior of kites and developing robust autonomous systems, but also for implementing more efficient design processes. For a lightweight membrane wing it is essential to take the strong fluid-structure coupling into account to achieve realistic simulation results. However, complex micro-scale Fluid-Structure Interaction (FSI) phenomena that are related to the low inertia of the wing such as canopy flutter have no important effects on the general flight dynamics. On the other hand, macro-scale FSI phenomena, such as wing torsion and bending induced by steering inputs, are large quasi-static wing deformations and can affect the flight dynamics significantly. Neglecting the effect of deformation such as in [6, 8, 9, 16] results in a model description of limited accuracy. Such models are typically used for trajectory optimization or basic controller design.

Recent research on highly flexible wings has employed particle-based approaches [7], multi-plate discretizations [15] and multibody discretizations [2] to capture the deformation behavior of the wing. However, such severe idealizations require fitting to empirical data which limits the prediction capabilities. On the other hand, high-

Fig. 17.1 High-resolution FE model of a Leading Edge Inflatable (LEI) tube kite [14]. This model uses over 30,000 elements for the wing and bridle system, includes all pulleys and accounts for the material properties of the fabric membranes and bridle lines and the pressurization of the tubes. It is based on the airbag solver of the MADYMO crash simulation software package and does not account for the aerodynamic load distribution resulting from an exterior flow.

resolution Finite Element approaches such as depicted in Fig. 17.1 are too detailed for most purposes and correspondingly too expensive in terms of CPU time. Furthermore, fast and accurate aerodynamic load models that match the level of detail of such an FE model do not exist at present.

A coupling of an FE wing model and a Vortex-Lattice Method (VLM) is used in [4] to describe the static deformation of a ram-air wing in flight. Since the VLM is based on the potential flow assumption the decisive effect of viscosity is not taken into account and the estimated aerodynamic surface pressure distribution is only of limited practical value. Subsequent work by [11] uses empirical corrections to capture at least some of the more important viscosity effects, such as flow separation.

There is still need for dynamic kite models that give a better physical representation of the flexible membrane wing and are well-balanced with respect to prediction quality, accuracy and computational speed. This chapter presents a fast and reasonably realistic approach for the flight dynamic modeling of LEI tube kites including superimposed aeroelastic phenomena that occur on the flight dynamic time scale. A model description is developed in Sect. 17.2 that includes all the macro-scale dynamic phenomena and quasi-static wing deformations, accepts steering line actuations as input and translates them via a mechanistic model to a dynamic response of the system. Micro-scale effects such as fluttering of the canopy are not considered. Section 17.3 demonstrates some simulation results leading to several conclusions in Sect. 17.4.

17.2 Computational model

This section describes the general modeling strategy followed by a description of the individual components and time integration strategy.

17.2.1 General strategy

The model architecture, as illustrated in Fig. 17.2, maps the structure of the physical problem, distinguishing a structural model to resolve the large-scale quasi-static deformation of the wing, an aerodynamic model to determine the quasi-steady distributed wing loading and a dynamic system model to describe the flight dynamics. Under nominal operational conditions the inertial forces of the wing are very small compared to the aerodynamic forces, since the wing is made from a very thin membrane. Also the micro-scale dynamics of the canopy are not of interest. Therefore the dynamics of the deformation of the wing are neglected, which results in a quasi-static FSI model.

The FE formulation of the wing structural model captures the static deformation response due to the aerodynamic load and the steering actuations. A nonlinear analysis is performed to compute finite displacements. To avoid the added complexity

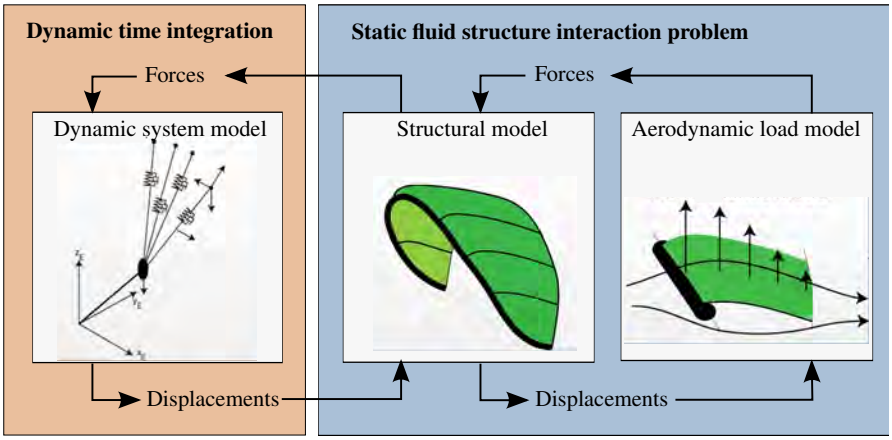

Fig. 17.2 Schematic of the kite modeling approach.

of inflated pressurized membrane tubes the inflatable leading edge and struts are represented as regular beam elements with nonlinear material properties. As a consequence, wrinkling effects are not considered. This is in line with the hypothesis of neglecting micro-scale effects. These start to have a considerable effect when the beam is bent strongly and eventually buckles. However, these extreme deformations occurring in off-design operational conditions and potentially leading to collapse of the wing are not considered in the analysis.

The static aerodynamic model of Breukels [2], Breukels and Ockels [3] is selected for computing the distributed aerodynamic load. This approach matches the level of detail of the structural model and is computational less intensive than the VLM or Computational Fluid Dynamics (CFD).

The dynamics of the system (wing, cables and KCU) are modeled with a simple system model that contains only the essential characteristics to demonstrate the modeling approach. At each time step the structural model of the wing provides forces to the dynamic system model that are applied to the end points of the cables where the wing is attached. The newly obtained positions of these cable attachment points after time integration are returned as displacement boundary conditions to the structural model. The lumped inertia of the wing is included in the dynamic system model by attaching point masses to the end of the cables.

This approach basically filters the high frequency (micro-scale) dynamics in the wing, but will show the wing deformations and dynamic effects in the global system that have a time constant much larger than the local dynamics of the wing. Effectively, the FSI problem quasi-statically follows the flight dynamics through the interface displacements applied as boundary conditions.

This method features several advantages. Micro-scale dynamic effects are not included which speeds up the simulation because no dynamic nonlinear FE analysis has to be performed, while all important macro-scale deformations and dynamics are present. Also, no large rotation kinematic model is needed, because the dynamic

model deals with the rigid body movements while the FSI model is written in a local frame and models only large displacements in the wing frame. It is also a flexible approach, because it is easy to replace individual components with different ones or use multiple software packages together.

More details on the used numerical techniques are described in [1].

17.2.2 Static structural wing model

The static nonlinear FE equations as derived from the potential energy equation state that the internal stiffness forces **f** should equal the external aerodynamic forces **g**.

$$\begin{cases} \mathbf{f}(\mathbf{q}) = \mathbf{g}(\mathbf{q}, \mathbf{X}) \\ \mathbf{q}_0, \mathbf{q}_b, \mathbf{X} \qquad \textit{prescribed} \end{cases} \tag{17.1}$$

with $\mathbf{q}$ the nodal displacements, $\mathbf{X}$ the dynamic system state that contains the wing velocity $\mathbf{V}_k$, the rotational wing velocity ω_k, and the wind velocity $\mathbf{V}_w$. The initial configuration $\mathbf{q}_0$ is prescribed by the structural solution from the previous time step. The boundary conditions $\mathbf{q}_b$ contain the prescribed degrees of freedom at the cable attachment points, computed by the dynamic simulation.

The nonlinearities are a result of the large displacements that cause a coupling between the bending and stretching of the FE elements, the configuration dependent stiffness of the inflatable beams and the nonlinear aerodynamic loading model.

The nonlinear quasi-static FSI equations have to be solved in an iterative manner. The Newton-Raphson scheme is used to solve the displacements of the FE wing model while the aerodynamic forces are held constant. After convergence of this structural loop the aerodynamic forces are updated in the aerodynamic loop and the structural displacements are recalculated for the new aerodynamic load. This continues until both loops have converged. An outer loop gradually increases the loads to the structure to create a more robust algorithm and speed up the calculations. A detailed description of this solution procedure is described by [1].

The kite that is modeled is the North Rhino 16 m^2 as depicted in Fig. 17.3 (right). This kite was chosen, because it contains all the essential features without having unnecessary complicated parts as a bridle system with pulleys or a double curved leading edge. The North Rhino is a C-shaped kite with an inflatable leading edge and five inflatable struts. The tips contain thin stiff beams and four attachment points for the lines. The trailing edge embeds a thin wire to prevent over-stretching and flapping of the trailing edge. The canopy is stitched to the top of the leading edge and struts and made from thin ripstop material.

Figure 17.3 (left) shows the global dimensions and used mesh of the undeformed and unloaded kite. A relatively coarse mesh is used to model the global deformations and to obtain short calculation times. A finer mesh is used in the tip areas, because those are subjected to the largest deformations and have the most influence on the

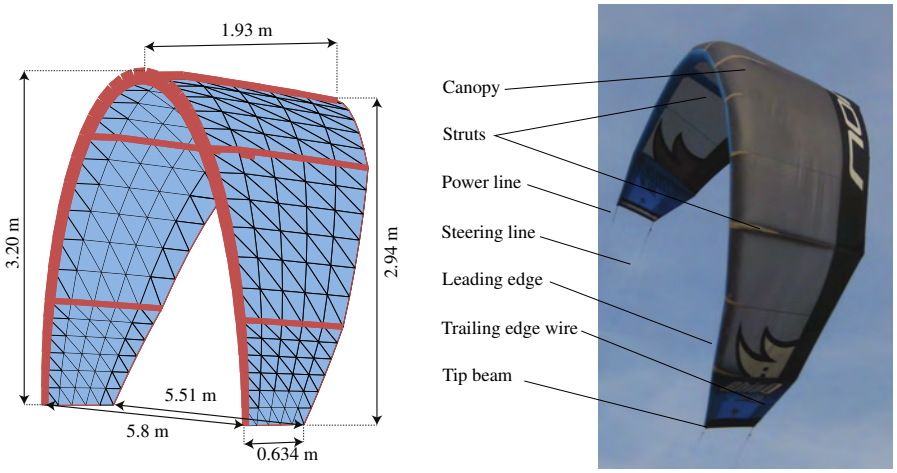

Fig. 17.3 Dimensions of the simulation model (left) and physical components (right) of the commercial North Rhino 16 m^2 kite.

steering behavior. To simplify the model it is assumed that the canopy is attached to the middle of the leading edge and struts instead of attached to the top.

Non-linear beam elements were developed to model the inflatable struts and leading edge. These elements are also used to model the trailing edge wire and tip beam. The material properties are obtained from experiments with inflated beams with different internal pressures and diameters, performed by Breukels [2]. This resulted in the bending stiffness $EI(p,v,r)$ depending on the pressure p, deflection v and radius r. The canopy is modeled with nonlinear three node triangular flat shell elements. The ripstop material is modeled as isotropic linear material with a Young's modulus of 1250 MPa, a Poisson ratio of 0.3 and a thickness of 0.08×10^{-3} m.

This all leads to the model properties as displayed in Table 17.1.

Beam elements	Shell elements	Nodes	DOF
107	360	222	1332

Table 17.1 FE properties of the wing

17.2.3 Steady aerodynamic wing loading model

The aerodynamic load model as described in [2, 3] and outlined in Chap. 16 is implemented according to the finite strip approach, which is based on the assumption that the aerodynamics of the wing can be approximated by modeling the wing as an

assembly of a finite number of connected two-dimensional single membrane airfoils in the spanwise direction. The aerodynamic load for each of these wing sections is determined separately, depending on its shape, angle of attack α and apparent wing velocity $\mathbf{V}_a$. The shape of a wing section is described by the chord length c, the camber $\kappa = b/c$, the thickness $t = d/l$ and the width w of a wing section as depicted in Fig. 17.4. This model only accounts for the steady-state aerodynamics and not the aerodynamics associated with the deformation speed of the wing or the added mass effect due to acceleration of the air. This is in line with the fact that the structural wing model is treated quasi-statically.

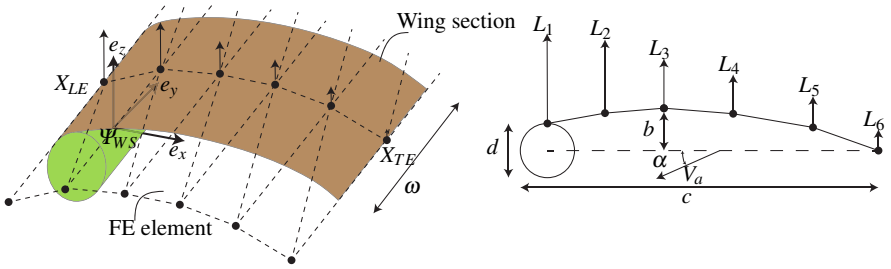

Fig. 17.4 A perspective view (left) and a side view (right) of a wing section.

Various values of these parameters (κ,t,α) served as input for CFD simulations of a two dimensional airfoil. The obtained pressure distributions for each set of parameters were related to a lift coefficient C_L, a drag coefficient C_D and an airfoil moment coefficient C_M. A fitting procedure resulted in three functions to map $\kappa,t,\alpha \rightarrow C_L,C_D,C_M$. From these coefficients, the resultant lift and drag force and airfoil moment can be calculated with conventional airfoil theory.

Each aerodynamic wing section is divided into a finite number of chordwise subsections by n nodes to distribute the total aerodynamic forces over the surface of the wing as shown in Fig. 17.4. The total lift and drag force are distributed over these nodes using a varying weighted approach that maintains the same airfoil moment of the wing sections resulting in the forces L_i on the nodes. Breukels [2] obtained the weight factors by comparing the overall aerodynamic forces for a strip resulting from this procedure with the original CFD data and selecting the best matching set.

The aerodynamic coefficients for each wing section are corrected for three dimensional aerodynamic effects based on an analysis of the variation of the lift coefficient along the span of the wing with the Vortex Lattice Method. This correction has not been included in this work, because the basic algorithm provides accurate enough information to demonstrate the feasibility of the modeling strategy.

The wing sections are defined such that a row of chordwise FE nodes defines the middle line of a wing section, so that the FE nodes overlap with the aerodynamic nodes as depicted in Fig. 17.4. The aerodynamic forces L_i can now easily be mapped to the FE structure. All the necessary parameters to calculate the wing section load can be directly derived from the positions of a chordwise row of FE nodes.

17.2.4 Dynamic system model

The dynamic model consists of the steering lines, power lines, tether, KCU, lumped wing mass and the forces that act on these components as depicted in Fig. 17.5 (left). All the components are modeled with a minimum amount of degrees of freedom.

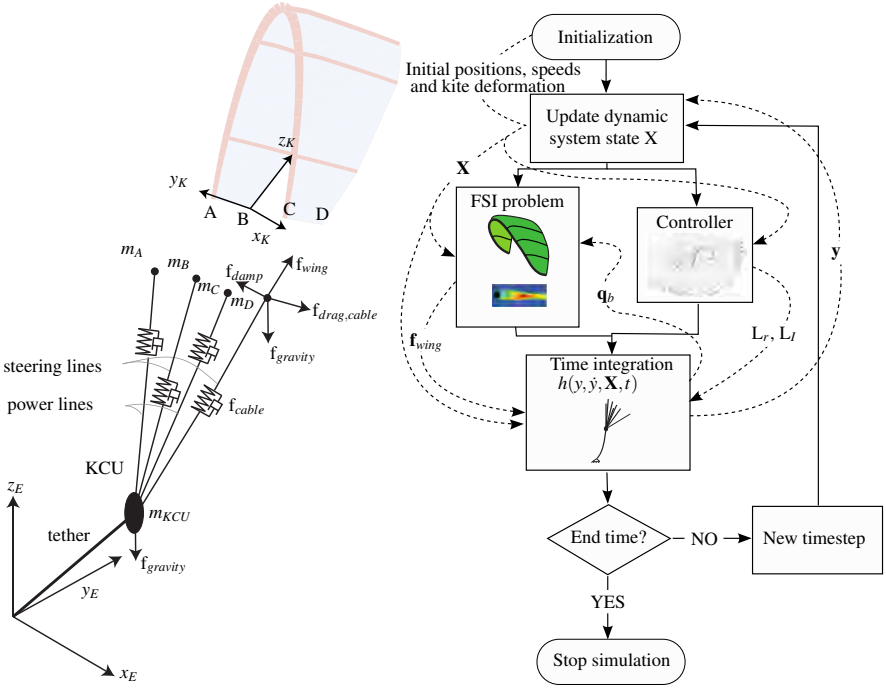

Fig. 17.5 The dynamic system model with the force components shown for one steering line (left). The models numerical integration process (right).

The steering and power lines need to be able to vary in length to give the wing the freedom to deform, since the change in their length and force are significant during steering movements [2]. Because the diameter is small (1.2 mm), lengths short and the mass low, the sag due to gravity is neglected. Therefore, these lines are modeled as linear spring-damper elements with constant spring and damper coefficients. This also allows for controlling the lengths of the steering lines by varying the unstretched spring lengths.

The tether has a larger diameter and is much heavier and therefore plays an important role in the system dynamics. However, the effects remain small during crosswind flights with a tether length up to 100 m [2]. Since the focus of this work is not on the tether dynamics, it is neglected and the tether is modeled as a distance constraint of 100 m.

The inertia of the wing is incorporated by distributing its mass over the end points of the lines (A,B,C,D). The mass effect can not be neglected in the global model as was done in the structural wing model, because the total mass of the wing is significant compared to the other components. The structural wing model exerts forces on these mass points. The accuracy of this method complies with the fact that the aerodynamic effects and not the inertial effects dominate the dynamic behavior of the system. Most of the mass is located at the leading edge side of the wing, therefore the power lines get 70% and the steering lines 30% of the total mass of the wing. The KCU is also represented by a point mass.

The global added mass effect due to the fact that the air has to be accelerated by the wing is neglected. Generally speaking this effect might not be negligible, but globally speaking the effect is small since the overall acceleration normal to the kite is small in practice and even zero in direction parallel to the tether when flying with a constant tether length.

The stiff beam in the wing tip of the structural model between points A-B and C-D will cause high frequent behavior in the dynamic model, but the displacements in this direction are very small. To improve the stability and speed of the dynamic model, a distance constraint is imposed between points A-B and C-D that eliminates this high frequent behavior without having a significant influence on the results.

The forces acting on the system are shown for one steering line in Fig. 17.5 (left) and consist of the gravity force $\mathbf{f}_g$, the wing force $\mathbf{f}_{wing}$ that comes from the structural model and the aerodynamic drag force $\mathbf{f}_{drag,cable}$ of the cable. Aerodynamic damping forces $\mathbf{f}_{damping}$ are introduced between the tips of the wing to represent the aerodynamic damping that is not taken into account in the structural model due to its static nature.

The resulting system has 12 degrees of freedom and can be described by the same number of generalized coordinates $\mathbf{y}$. The equations of motion are set up using the TMT method [13] that uses a combination of independent generalized coordinates, virtual power and an inertia contribution via d'Alembert forces. This results in the equations of motion

$$\bar{\mathbf{M}}\ddot{\mathbf{y}} = \bar{\mathbf{f}} \tag{17.2}$$

with the generalized mass matrix $\bar{\mathbf{M}}$ and the generalized forces $\bar{\mathbf{f}}$.

Numerical time integration

The differential equations of the dynamic model can be written in the form

$$\ddot{\mathbf{y}} = \mathbf{h}(\mathbf{y}, \dot{\mathbf{y}}, \mathbf{X}, t) \tag{17.3}$$

where $\ddot{\mathbf{y}}$ are the accelerations related to the degrees of freedom $\mathbf{y}$, the time derivatives $\dot{\mathbf{y}}$ and the dynamic state of the system $\mathbf{X}$ which contains the wing velocity $\mathbf{V}_k$, the rotational wing velocity ω_k, and the wind velocity $\mathbf{V}_w$. Information between the dynamic simulation and FSI analysis is shared via the kite reference frame K as

depicted in Fig. 17.5 (left). The movement of K describes the flight dynamics of the wing.

Equation 17.3 can be rewritten in the form of a standard system of two first order differential equations

$$\begin{bmatrix} \dot{\mathbf{y}} \\ \dot{\mathbf{u}} \end{bmatrix} = \begin{bmatrix} \mathbf{u} \\ \mathbf{h}(\mathbf{y}, \dot{\mathbf{y}}, \mathbf{X}, t) \end{bmatrix} \tag{17.4}$$

Figure 17.5 (right) shows the flow chart of the system with all the components. During the initialization phase all the parameters and initial variable values are set. The dynamic system state $\mathbf{X}$ is recalculated during the system state update phase. The FSI problem receives the cable attachment point displacements $\mathbf{q}_b$ as boundary conditions and the system state $\mathbf{X}$ and returns the forces $\mathbf{f}_{wing}$ that are applied to the cable attachment points in the dynamic simulation. A steering controller based on the work of Jehle and Schmehl [9] stabilizes the kite and steers it into a desired trajectory by adjusting the line lengths of the steering lines L_r and L_l. They are given as an input to the dynamic equations. A force controller also adjust the lengths of the steering lines to control the pitch angle of the wing. In this way the total lift force in the wing can be controlled to prevent it from stalling or collapsing. This controller is not used in the physical system, because there the tether reel-out speed controller is used for this purpose. A numerical solver performs the time integration by solving the dynamic equations several times to calculate the new value of the degrees of freedom $\mathbf{y}$. When the new vector $\mathbf{y}$ has been determined, the algorithm proceeds with the next time step.

The forces calculated by the FSI problem depend on $\mathbf{y}$ and $\mathbf{X}$ and are therefore actually part of the dynamic equations that calculate $\ddot{\mathbf{y}}$. Every dynamic solving algorithm needs multiple dynamic function evaluations to calculate the positions $\mathbf{y}_{n+1}$ in the next time-step. Since the most computational intensive part in this modeling approach is to solve the FSI problem, it would result in a very slow time integration algorithm if the FSI problem has to be solved for every time the accelerations $\ddot{\mathbf{y}}$ are being calculated.

Therefore a staggered approach is used where the forces coming from the FSI model of the wing are computed at time t_n and then used to advance the dynamic model from t_n to t_{n+1}, without computing the forces at t_{n+1}. This allows uncoupling the nonlinear force computation from the dynamic integration and is acceptable for small time steps. The FSI problem now only has to be solved once per time step. This will greatly speed up the numerical algorithm.

The choice of solving algorithm remarkably affects the computational time. Implicit time-integration algorithms show better stability and can take larger time-steps at the cost of more function evaluations. Since the FSI problem was removed from the function and the dynamic function evaluation is now computationally cheap, an implicit solver seems to be the appropriate choice. However, the relation between step-size and speed is not that trivial. A larger step-size means a larger difference between the wing configurations in two subsequent time steps which results in more iterations during the FSI solving procedure. Since this is the most computational in-

tensive part, it might be more advantageous to use an explicit solver with a smaller step-size. It is indeed observed that the explicit Runge-Kutta(4,5) integrator [5] as implemented in the ODE45 Matlab® function is the fastest algorithm to solve the equations [1].

17.3 Results

The described computational model and the flight controller have been implemented in Matlab®. The representative figure eight trajectory depicted in Fig. 17.6 was selected for the analysis. The kite starts in the center at point P_0 and travels via $P_i, i = 1, ..., 4$. These same points are shown on the upper horizontal axis in all the following results graphs. A small offset between the desired and actual trajectory can be observed especially in the lower parts, which is a result of the basic steering controller algorithm with only a proportional part.

The code was programmed in Matlab® and was run on a computer with an Intel core i5 750 @ 2.8GHz and 4GB memory. Tests with several solvers showed that the explicit Runge-Kutta(4,5) algorithm with a variable time step was by far the fastest, resulting in a speed that is 27.5 times slower than real-time. The solver used an average step-size of 5.3 milliseconds.

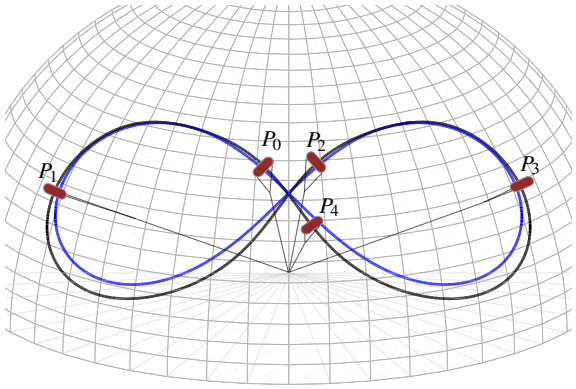

Fig. 17.6 Crosswind figure eight flight of 20s, blue: desired trajectory, black: actual trajectory.

17.3.1 Steering behavior

An important reason to incorporate the inherent flexibility of the wing is to analyze the aeroelastic phenomenon that determines the steering behavior.

Let a left turn be defined as a movement to the right seen from an observers perspective on the ground controlling the kite. The left steering line is connected

to the left wing tip. According to Breukels [2], the angle of attack at the right tip of the wing increases and of the left tip decreases when the wing is steered to the right as a result of a steering line length difference. This results in a higher drag force on the right tip that creates a yawing moment. The lift force on the right tip also increases compared to the left tip. Together with the torsional deformation of the wing, this also creates a yawing moment. The higher force on the right steering line causes the right tip to bend forward towards the leading edge and the left tip to bend backward as shown in Fig. 17.7 (left). The deformation of the wing results in an offset between the working line of the lift forces on both tips, creating a yawing moment that makes the kite turn. This knowledge forms a basis to verify the steering results of the developed kite model in this section.

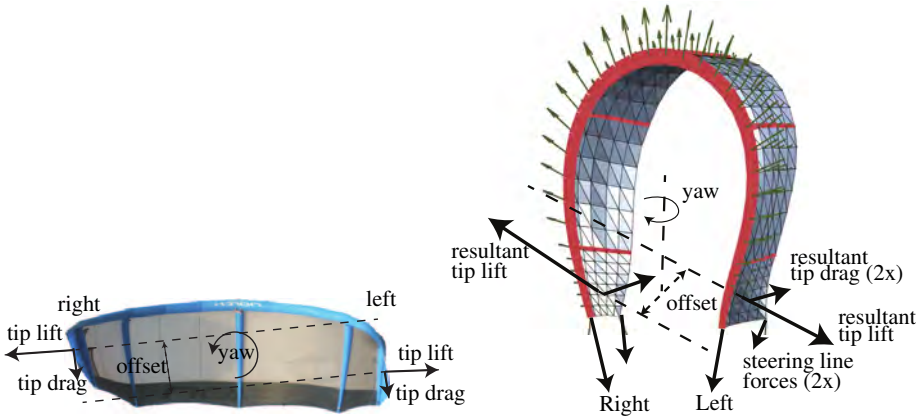

Fig. 17.7 Bottom view of the wing torsion due to a right steering input (left), simulated shape response (magnified displacements) to a right steering input (right).

Figure 17.7 (right) shows the deformation of the wing model while cornering. The torsional deformation as discussed above can clearly be seen and is similar to Fig. 17.7 (right).

Figure 17.8 shows that the angle of attack increases on the right tip and decreases on the left tip while steering to the right and vice versa. The angle of attack at the left tip even becomes negative for a while. The higher angle of attack results in a higher lift and drag force at the right tip. This is exactly what was expected and described by Breukels. Some oscillations can be seen at the tip sections right after passing point P_1. This is the result of a fast increase in the steering input to be able to follow the trajectory. The angle of attack of the left tip becomes negative here. Switching from a positive to a negative angle of attack, causes the sign of the lift force to flip. This results in some oscillations. Similar oscillations have been seen at the tips in the real system.

Figure 17.9 shows how the steering input relates to the yaw rate of the kite. A line length difference of the steering lines results in a yawing motion in the correct direction, as was expected. A relation between yaw rate and controller steering input

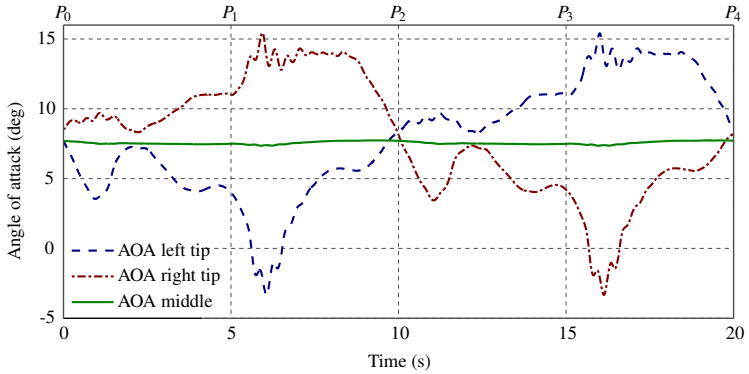

Fig. 17.8 Angle of attack of the left tip, right tip and middle section of the wing.

is observed. This proportional relationship was also found before by Erhard and Strauch [6] and Jehle and Schmehl [9] from separate experimental datasets and is a confirmation of the model plausibility.

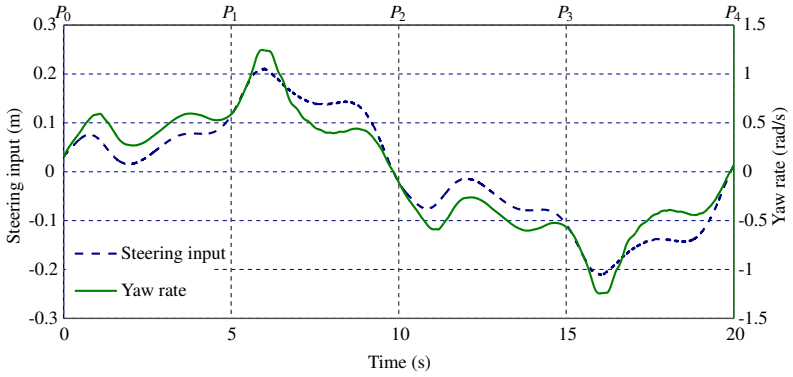

Fig. 17.9 Relation between the steering input and yaw rate.

17.3.2 Aerodynamics

Measured L/D values with the test system show values around 6 for a similar type of kite [12], which is slightly lower than the value between 7.5 and 9 that the simulations show. As a consequence the flight speeds are higher than expected, since they vary linearly with the L/D ratio [10].

Multiple explanations can be pointed out. Firstly, the aerodynamic model underestimates induced drag effects from three-dimensional flow phenomena such as tip-

vortices. Secondly, the modeling assumption in the structural model that the canopy is not attached to the top of the leading edge, but connected to its center, results in substantially lower values of the camber of the wing sections. This reduces the drag more significantly than the lift, resulting in a higher L/D. This should be corrected in future structural models. Furthermore, the structural model is slightly stiffer than the real wing due to the used coarse mesh, resulting in less deformation of the canopy and a smaller camber.

Future work should include a study of the effect of unsteady flow conditions on the aerodynamic forces. Changes in aerodynamic forces due to the deformation speed of the wing and the added mass effect due to the fact that the wing has to accelerate air, are not accounted for in the steady-state model.

The aerodynamic model is the main source of uncertainties in this modeling study. It ignores several three-dimensional effects, shows peculiarities in the aerodynamic lift, drag and airfoil moment curves and uses an approximate method to distribute the aerodynamic load over the wing surface. The deformation and flight velocities of the wing both fully depend on the forces produced by the aerodynamic model. Therefore, much can be gained from improving the aerodynamic loading model in future work. However, it suffices to be used in this first attempt to demonstrate the feasibility of the computational strategy.

17.3.3 Structural deformation

Next to the torsion occurring during steering the wing exhibits additional characteristic macro-scale deformation modes. Figure 17.10 shows the displacements of the four line attachment points in the transverse direction of the kite reference frame. It can be seen that points A and B move to and from point C and D. This phenomenon occurs also in reality and is sometimes referred to as *jellyfishing* or bending of the wing as shown in Fig. 17.11.

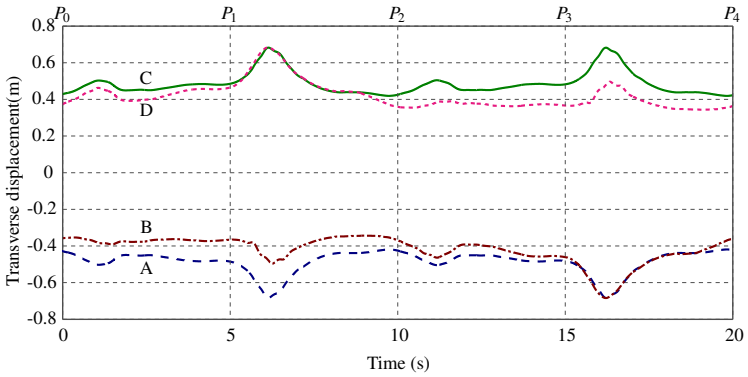

Fig. 17.10 Transverse displacements of the line attachment points.

The maximum transverse deformation of each tip is approximately 0.7 meters compared to the undeformed structure, resulting in a total variation of the tip distance of 1.4 m. This is almost 25% of the wing span, which clearly indicates the necessity of a nonlinear modeling approach.

The transverse displacement variations during steady flight are smaller. Each line attachment point stays within a region of 0.3 m and in the simulation the wing does not show severe oscillations. Similar behavior can be observed in flight tests. Even though an inflatable structure is very flexible, the aerodynamic loading puts the structure under tension such that it becomes very stiff. The flexible behavior reveals itself during sudden wind gusts resulting in severe variations of the wing loading. Since the model uses a constant wind field, such behavior was not expected to show up, but is an interesting research case for future work.

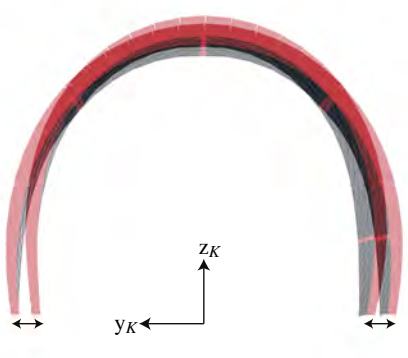

Fig. 17.11 Jellyfishing/bending mode of the wing (frontview).

17.4 Conclusions

This chapter demonstrates the feasibility of a computational approach to model flight dynamics and aeroelastic phenomena of LEI kites used in AWE-systems. The approach combines a quasi-static nonlinear FE structural wing model with a static empirical aerodynamic loading model to capture the fluid-structure-interaction. The resulting forces serve as input to a dynamic system model that describes the flight dynamics. The wing inertia are neglected in the static FSI analysis, because mainly the macro scale deformations and dynamics determine the flight behavior.

Results show that the model produces the same important macro-scale bending and torsion modes of the wing that are seen in real wings when flying a crosswind trajectory. Large deformations are observed, showing the necessity of performing a nonlinear analysis. The torsional deformation is the result of changing the relative length of the steering lines and results in a realistic steering movement of the kite.

The relation found between the yaw rate and steering input is qualitatively very similar to what is described in researches based on experimental data.

It is shown that the simulation is fast considering the complexity of the problem that is solved and the Matlab®implementation. Neglecting the dynamics related to the wing inertia in the FSI-problem greatly reduces the computational time, since the time-integration in the model only has to be performed on the limited degrees of freedom in the dynamic system model instead of thousands degrees of freedom in the structural model. Simplifying the structural model by using regular beam elements for the inflatable beams also reduces the computational time and still produces plausible deformations.

The important limiting factor in this modeling approach is the accuracy of the aerodynamic loading model. All model results depend on the input from this model. This doesn't restrict the feasibility of the modeling strategy, since the aerodynamic model can be replaced by a different one in future work. However, currently no better models exist that match the same level of detail and speed, but are under development at this moment. Future work should also include a full validation of the computational modeling approach.

Concluding, it can be said that the developed strategy is very promising for future work and fosters a new generation of kite models that helps improving the AWE systems.

Acknowledgements The financial support of the Rotterdam Climate Initiative is gratefully acknowledged. The authors would like to thank Claudius Jehle for contributing the concept of the implemented autopilot.

References

1. Bosch, H. A.: Finite Element Analysis of a Kite for Power Generation. M.Sc.Thesis, Delft University of Technology, 2012. http://resolver.tudelft.nl/uuid:888fe64a-b101-438c-aa6f-8a0b34603f8e
2. Breukels, J.: An Engineering Methodology for Kite Design. Ph.D. Thesis, Delft University of Technology, 2011. http://resolver.tudelft.nl/uuid:cdece38a-1f13-47cc-b277-ed64fdda7cdf
3. Breukels, J., Ockels, W. J.: A Multi-Body System Approach to the Simulation of Flexible Membrane Airfoils. Aerotecnica Missili Spazio **89**(3), 119–134 (2010)
4. Chatzikonstantinou, T.: Numerical analysis of three-dimensional non rigid wings. AIAA Paper 89-0907. In: Proceedings of the 10th Aerodynamic Decelerator Conference, Cocoa Beach, FL, USA, 18–20 Mar 1989. doi: 10.2514/6.1989-907
5. Dormand, J. R., Prince, P. J.: A family of embedded Runge-Kutta formulae. Journal of Computational and Applied Mathematics **6**(1), 19–26 (1980). doi: 10.1016/0771-050X(80)90013-3
6. Erhard, M., Strauch, H.: Control of Towing Kites for Seagoing Vessels. IEEE Transactions on Control Systems Technology (2012). doi: 10.1109/TCST.2012.2221093. arXiv:1202.3641 [cs.DS]
7. Furey, A., Harvey, I.: Evolution of Neural Networks for Active Control of Tethered Airfoils. In: Advances in Artificial Life, Vol. 4648, Lecture Notes in Computational Science and En-

gineering, pp. 746–755. Springer, Berlin-Heidelberg (2007). doi: 10.1007/978-3-540-74913-4_75
8. Houska, B.: Robustness and Stability Optimization of Open-Loop Controlled Power Generating Kites. M.Sc.Thesis, Ruprecht-Karls-Universität, Heidelberg, 2007. http://www.kuleuven.be/optec/files/Houska2007a.pdf
9. Jehle, C., Schmehl, R.: Applied Tracking Control for Kite Power Systems. Accepted for publication in AIAA Journal of Guidance, Control and Dynamics (2013)
10. Loyd, M. L.: Crosswind kite power. Journal of Energy **4**(3), 106–111 (1980). doi: 10.2514/3.48021
11. Müller, S.: Modellierung, Stabilität und Dynamik von Gleitschirmsystemen. Ph.D. Thesis, TU Munich, 2002
12. Ruppert, M. B.: Development and Validation of a Real Time Pumping Kite Model. M.Sc.Thesis, Delft University of Technology, 2012
13. Schwab, A. L.: Multibody Dynamics B. Lecture Notes. 2002. http://bicycle.tudelft.nl/schwab/Publications/LinSch02.pdf
14. Schwoll, J.: Finite Element approach for statically loaded inflatable kite structures. M.Sc.Thesis, Delft University of Technology, 2012
15. Williams, P., Lansdorp, B., Ockels, W.: Flexible Tethered Kite with Moveable Attachment Points, Part I: Dynamics and Control. AIAA-Paper 2007-6628. In: Proceedings of the AIAA Atmospheric Flight Mechanics Conference and Exhibit, Hilton Head, SC, USA, 20–23 Aug 2007. doi: 10.2514/6.2007-6628
16. Williams, P., Lansdorp, B., Ruiterkamp, R., Ockels, W.: Modeling, Simulation, and Testing of Surf Kites for Power Generation. AIAA Paper 2008-6693. In: Proceedings of the AIAA Modeling and Simulation Technologies Conference and Exhibit, Honolulu, HI, USA, 18–21 Aug 2008. doi: 10.2514/6.2008-6693